# Chapter 1

# Waves in Non-neutral Plasma

François Anderegg
*University of California at San Diego, Physics Dept. 0319,*
*9500 Gilman Drive, La Jolla, CA USA,*
*fanderegg@ucsd.edu*

In this presentation, I will give an elementary introduction to plasma waves in single-species non-neutral plasmas. The plasma is presumed to be trapped in an elongated cylindrical trap with an axial magnetic field; this geometry is referred to as a Penning-Malmberg trap. The first part of the presentation is about low frequency drift waves called Diocotron waves, followed by plasma waves of two different types, and the last part of the presentation is about cyclotron waves, which are the highest frequency electrostatic waves in Penning-Malmberg traps.

## 1.1. Diocotron Waves

The word Diocotron comes from the Greek meaning "pursue, chase." Apparently in 1952 researchers conducting experiments with hollow electron beams inside a conducting cylinder in a magnetic field observed that hollow beams of charge were unstable. The beam broke apart, and the pieces were rotating around the magnetic field axis and "chasing" each other. They named that instability the Diocotron instability. A comprehensive review of diocotron instability can be found in Chapter 6 of *Physics of Non-Neutral Plasmas* by R. Davidson.[1] In this presentation, I will be describing stable Diocotron waves, not the diocotron instability observed on hollow electron beams. The properties of stable diocotron waves were first measured by deGrassie and Malmberg[2] in confined pure electron columns.

We will consider a simple case of a monotonically decreasing density profile of ions trapped in an elongated Penning-Malmberg trap. A simple intoduction to Penning-Malmberg traps can be found in a *Physics Today* article.[3] Figure 1.1 shows the trap geometry and the coordinates used. The

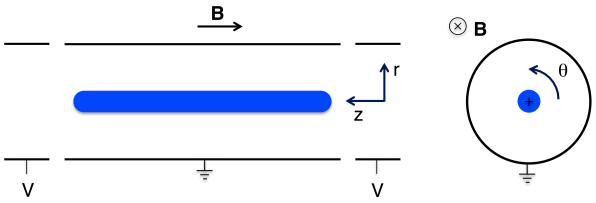


Fig. 1.1. Schematic of a Penning-Malmberg trap containing positive charges.

plasma is assumed to be "rigid," that is individual ions "bounce" rapidly along the magnetic field compared to their rotation around the axis of the trap. For low frequency drift waves, the rapid bouncing of the particles along the magnetic field axis averages any $z$-dependence, and we will assume here that Diocotron waves have no axial variation, i.e. $k_z = 0$.

### 1.1.1. *Infinite length description*

To start the description of the Diocotron wave, we will assume that the plasma column is "infinitely" long and that it can be described by a 2 dimensional model. In general the density perturbation has the form $\delta n = \delta n(r) \exp\{i(m_\theta \theta + k_z z - \omega t)\}$; here we will discuss the case of $m_\theta = 1$ and $k_z = 0$.

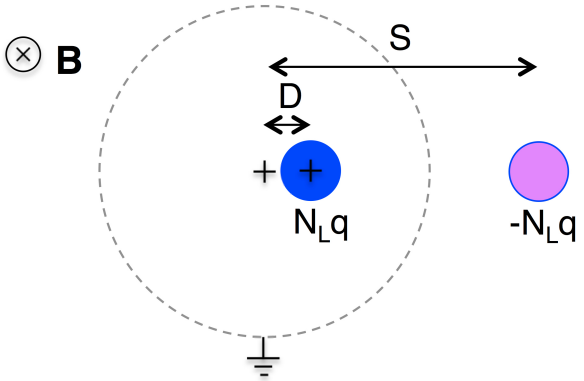


Fig. 1.2. Image charge model of the diocotron wave for an infinitely long line of charge.

Figure 1.2 shows an end view of a plasma column with line density

$N_L[m^{-1}]$ of particles with (positive) charge $q$, displaced from the axis by a distance $D$. We can replace the wall by an equal and opposite "image charge" located at a distance $S$ from the center of the trap such that the potential at $r = R_w$ is a constant: $\phi(R_w, \theta) = \text{const}$. From a symmetry argument, the image charge has to be located at the same azimuthal angle $\theta$ as the real charges. The potential from 2 infinitely long lines of charge is:

$$\begin{aligned}\phi(r,\theta) &= -\frac{N_L q}{2\pi\varepsilon_0}\left[\ln\sqrt{r^2+D^2-2rD\cos\theta} - \ln\sqrt{r^2+S^2-2rS\cos\theta}\right] \\ &= -\frac{N_L q}{2\pi\varepsilon_0}\ln\left[\frac{r\sqrt{1+\frac{D^2}{r^2}-\frac{2D}{r}\cos\theta}}{S\sqrt{1+\frac{r^2}{S^2}-\frac{2r}{S}\cos\theta}}\right] . \end{aligned} \tag{1.1}$$

By choosing $S/R_w = R_W/D$, that is, $S = R_w^2/D$, the potential at the location of the wall can be written as

$$\phi(R_W,\theta) = -\frac{N_L q}{2\pi\varepsilon_0}\ln\left(\frac{D}{R_w}\right) \tag{1.2}$$

which is independent of $\theta$. The electric field from a line of charge can be calculated using Gauss' Law:

$$E(r) = \frac{\sum Q}{2\pi\varepsilon_0 r L} = \frac{N_L q}{2\pi\varepsilon_0 r} \tag{1.3}$$

therefore the image charge electric field at $r = 0$ is:

$$E_i(r=0) = -\frac{N_L q}{2\pi\varepsilon_0 S} = -\frac{N_L q D}{2\pi\varepsilon_0 R_w^2}. \tag{1.4}$$

The $E \times B$ drift velocity $\mathrm{v}_d$ of the (real) charge in the electric field of the image charge is:

$$\mathrm{v}_d = \frac{E_i}{B} = -\frac{N_L q D}{2\pi\varepsilon_0 B_z R_w^2} \tag{1.5}$$

where we have assumed that the displacement $D$ is small ($D/R_w \ll 1$). The infinite length small amplitude Diocotron frequency is:

$$f_{\mathrm{dio}}^{\infty} = \frac{\mathrm{v}_d}{2\pi D} = \frac{N_L q}{4\pi^2\varepsilon_0 B_z R_w^2}. \tag{1.6}$$

From an experimental point of view, the diocotron mode frequency gives a measure of the line density $N_L$. We have to be careful here since the above equation is valid only for infinite length and small amplitude. If one measures the line density $N_L$ with a dump technique[4] and also measures the diocotron frequency for a column with $L_p \sim 2R_p$, the infinite length equation gives a frequency too small by a factor of up to 2 or 3.

We will describe later corrections to $f_{\rm dio}^{\infty}$ to include the effect of a realistic plasma, that is, finite amplitude, finite length, temperature shift, etc.

### 1.1.2. *A negative energy mode*

The diocotron mode is a negative energy mode. This can be easily seen in the image charge model that we have used in this presentation. The image charge has the opposite sign of the "real" charge, therefore as the plasma is attracted towards its image charge, the electrostatic energy decreases as the mode amplitude increases. Here any kinetic energy is ignored. Let's calculate how much electrostatic energy is required to displace the plasma by a distance $D$ in the image charge electric field.

$$W_{\rm ES} = \int_0^D Q \cdot E_i dx = \int_0^D N_L q L_p \left( \frac{-N_L q x}{2\pi\varepsilon_0 R_w^2} \right) dx$$
$$= -\frac{(N_L q)^2}{4\pi\varepsilon_0} \frac{D^2}{R_w^2} L_p < 0. \tag{1.7}$$

The electrostatic energy $W_{\rm ES}$ is negative; this means that the diocotron

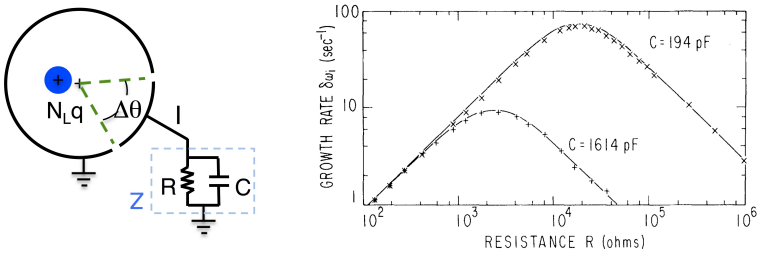


Fig. 1.3. Sectored electrode with model of impedance $Z$. Growth rate plotted versus resistance $R$.

mode can be destabilized by dissipation. This destabilization is referred to as "resistive growth." Figure 1.3 illustrates how an azimuthal section of the wall (called a sector) can destabilize the dioctron mode. The power dissipated in the load connected to the sector is $P = \frac{1}{2} I^2 \mathrm{Re}(Z)$, where $I$ is the image current, and the electrostatic energy in the wave is $W_{\rm wave}$.

Therefore the growth rate of the wave is:[5]

$$\gamma = \frac{P}{2W_{\text{wave}}} = \frac{4\varepsilon_0}{\pi}\frac{\omega^2 L_s^2 \sin^2\frac{\Delta\theta}{2}}{L_p}\text{Re}(Z) \tag{1.8}$$

for the RC circuit shown on Fig. 1.3 the real part of the impedance is

$$\text{Re}(Z) = \frac{R}{1+\omega^2 R^2 C^2}. \tag{1.9}$$

This growth rate was carefully verified experimentally[5] as shown on Fig. 1.3. As the external resistance $R$ is increased, the growth rate increases linearly up to a maximum corresponding to $\omega^2 R^2 C^2 = 1$; at the maximum growth rate, half of the current is flowing through the resistor and the other half through the capacitor. As $R$ is further increased, the growth rate is reduced since more and more current flows through the dissipationless capacitor. Figure 1.3 also shows the growth rate for a different capacitor, further validating the model. Figure 1.4 shows how a feedback circuit can

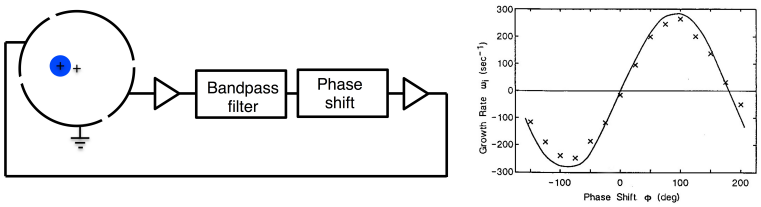


Fig. 1.4. Schematic of diocotron feedback circuit and feedback growth rate versus phase shift.

be used to damp a diocotron mode, by phase-shifting the sector voltage so as to obtain an effective "negative resistance." Changing the phase of the feedback controls the growth or damping rate of the diocotron mode.[6]

The diocotron mode provides a useful technique to control the position of the plasma in a trap. For example Fig. 1.5 shows a "phaser" pictures of $z$-integrated density obtained by multiple dumps and measuring the charge passing through a collimator hole at varying azimuthal positions of the plasma.[7] Also the diocotron mode is a good tool to load off axis multitrap cells[8] designed to store large numbers of particles such as positrons.

### 1.1.3. *Finite amplitude shift of diocotron mode*

For large displacement $D$, the plasma column distorts into an elliptical cross-section and the frequency of the diocotron mode increases, as[9]

$$f_{\rm dio} = f^{\infty}_{\rm dio} + f^{\infty}_{\rm dio}\left(\frac{1-2(R_p/R_w)^2}{[1-(R_p/R_w)^2]^2}\right)\left(\frac{D}{R_w}\right)^2. \qquad (1.10)$$

The measured amplitude shift versus normalized displacement is shown on

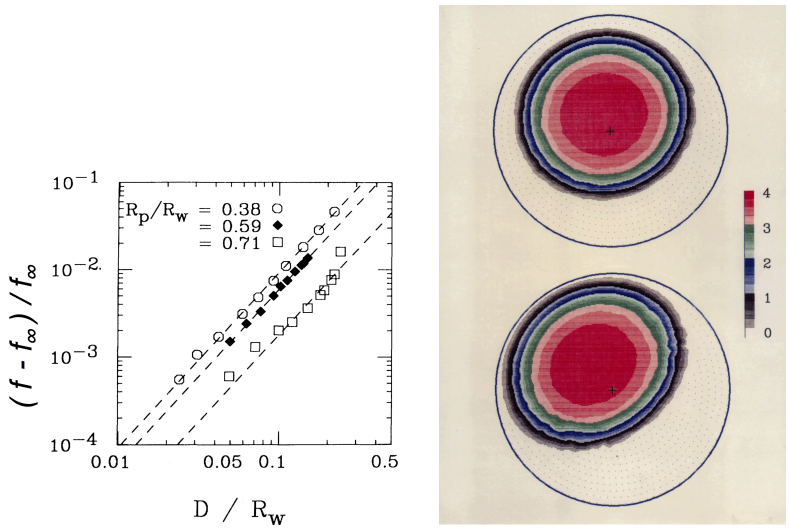


Fig. 1.5. (a) Measured frequency shift vs. amplitude for three different radius plasmas. (b) "Phaser" picture of $z$-integrated density; colors represent density on a linear scale of $10^6\mathrm{cm}^{-3}$, showing elliptical distortion of the plasma for large displacement.

Fig. 1.5 for 3 different plasma radii. Figure 1.5b shows phase-locked densities $n(r,\theta)$ for the diocotron at two amplitudes showing elliptical distortion; for both cases $R_p = 2.42$cm and the wall radius was at $R_w = 3.81$cm.

### 1.1.4. *Finite length diocotron*

The confining potential at the end of the trap pushes the plasma in the $z$-direction, resulting in a radial force on an off-axis plasma. The force comes from the radial component of the confining potential and adds to the force due to the image charge. $F_{\rm tot} = F_i + F_c$ where $F_i$ is due to the image and $F_c$ is due to the confinement. A careful calculation of the frequency change

has been conducted[10] and gives:

$$\frac{f_{\rm dio}}{f_{\rm dio}^{\infty}} = \frac{F_{\rm tot}}{F_{i,\infty}} = 1 + \left[\frac{j_{01}}{2}\left(\frac{1}{4} + \ln\left(\frac{R_w}{R_p}\right) + \frac{k_B T 4\pi\varepsilon_0}{N_L e^2}\right) - 0.671\right]\left(\frac{R_w}{L_p}\right). \tag{1.11}$$

The plasma electrostatic pressure (term: $\frac{1}{4}+\ln(R_w/R_p)$) pushes on the end confining potential, increasing the diocotron frequency. The plasma kinetic pressure [term: $k_B T 4\pi\varepsilon_0/(N_L e^2)$] also similarly increases the frequency. Finally the finite length of the image charge reduces the force (term 0.671); the numerical factor comes from the specific shape of the vacuum potential of cylindrical electrodes. The finite length diocotron frequency equation has been extensively tested experimentally.

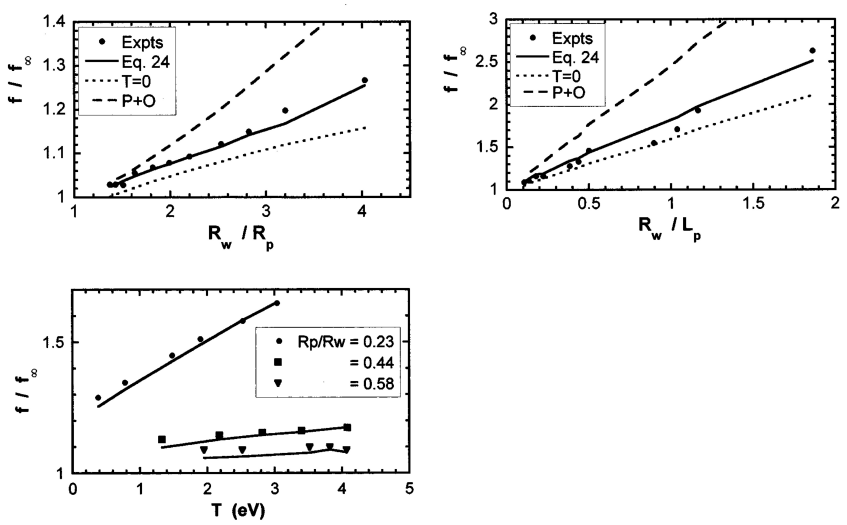


Fig. 1.6. Measured diocotron frequency versus plasma radius, plasma length, and temperature showing agreement with Eq. (1.11). The long dashed line is a theory for "non-rigid" plasmas.[11]

Figure 1.6 shows the measured frequency shift plotted against $R_w/R_p$ and $R_w/L_p$. In both cases the solid line is the theory prediction of Eq. (1.11) with no adjustable parameters. The kinetic pressure term $k_B T 4\pi\varepsilon_0/(N_L e^2)$ can also be written as $4\lambda_D^2/R_p^2$; it is small for plasmas which have many Debye lengths across, but it is large for clouds made out of a few particles with a large Debye length. The third graph of Fig. 1.6 shows the measured

kinetic pressure shift for 3 different plasma radii. Note that the kinetic pressure shift is much larger for small plasmas (large $\lambda_D/R_p$) than for large plasmas. These finite length corrections are important to account for when using the diocotron frequency to measure the line density.

### 1.1.5. *Magnetron regime*

For short and low density plasmas, the radial component of the confinement potential is substantially larger than the potential due to the image charge. In this regime the "diocotron mode" is called the "magnetron mode." In this regime the frequency of the mode is almost independent of the amount of charge in the trap, contrasting sharply with the diocotron mode described before. The frequency of the mode is:[10]

$$f = -\frac{E_r}{2\pi D B_z} = \frac{1}{2\pi D B_z}\left[\frac{\partial \phi_c}{\partial r} + \frac{\partial \phi_i}{\partial r}\right]_{r=D} \tag{1.12}$$

where $\phi_c$ is the confinement potential and $\phi_i$ is the potential due to the image charge. For a cylindrical trap with a trapping electrode length $L$ and a confining potential $V_c$ applied to the end of the trapping electrode, one gets[10]

$$f = \frac{1}{2\pi B_z}\left[\underbrace{1.15\frac{V_c}{R_w^2}\frac{L}{R_w}}_{\text{magnetron}} - \underbrace{1.0027\frac{Q}{R_w^3}}_{\text{diocotron}}\right]. \tag{1.13}$$

For example, $10^5$ electrons contained in a trap with $V_c = 10$V, $R_w = 1$cm, $L/R_w = 0.2$, the magnetron term is 230 kHz and the diocotron term is 1.4 kHz.

### 1.1.6. *Higher order diocotron modes*

The image charge model we have used so far has the advantage of giving a physical intuition of the dioctoron mode but is limited to $m_\theta = 1$. The standard linear theory of diocotron modes can be found in Refs. 11 and 1, giving a diocotron mode frequency:

$$f_{\text{dio}}^{m_\theta} = f_{E\times B}\left[m_\theta - 1 + \left(\frac{R_p}{R_w}\right)^{2m_\theta}\right] \tag{1.14}$$

where $f_{E\times B}$ is the plasma rotation frequency and $m_\theta$ is the azimuthal mode number. For a square profile $f_{E\times B} = qn/(4\pi\varepsilon_0 B)$. For $m_\theta = 1$ this result is

identical to the image charge model for infinite length and small amplitude, Eq. (1.6).

One can see from Eq. (1.14) that for the $m_\theta = 1$ mode, the diocotron frequency is the plasma rotation frequency reduced by $(R_p/R_w)^2$. Also for a small radius plasma, the $m_\theta = 2$ diocotron frequency is almost at the plasma rotation frequency.

### 1.2. Plasma Waves

We are considering a long plasma in a conducting cylinder with a magnetic field $B$ aligned with the trap axis. The magnetic field is strong enough to make the cyclotron frequency much larger than the plasma frequency, but the exact magnitude of the magnetic field is not important.

To derive the frequency of plasma waves in a trap, we start by writing the continuity equation,

$$\frac{\partial n}{\partial t} + \frac{\partial}{\partial z} n \cdot \mathrm{v}_z = 0 \tag{1.15}$$

and Newton equation

$$m \frac{\partial \mathrm{v}_z}{\partial t} = qE_z = -q \frac{\partial}{\partial z} \phi. \tag{1.16}$$

Note that we have kept only the $z$ dynamics in these two equations, but we will keep all components for the Poisson equation:

$$\nabla^2 \phi = -4\pi q \delta n. \tag{1.17}$$

We will now assume that the density perturbation is $\delta n(r) \exp\{i(m_\theta \theta + k_z z - \omega t)\}$, and the above equations become

$$-i\omega \delta n + n\, ik_z \delta \mathrm{v}_z = 0; \tag{1.18}$$

$$-mi\omega \delta \mathrm{v}_z = -qik_z \delta\phi; \tag{1.19}$$

$$-k^2 \delta\phi = -4\pi q \delta n. \tag{1.20}$$

Combining these 3 equations, one gets the Trivelpiece-Gould[12] mode dispersion relation for a cold plasma,

$$\omega^2 = \frac{k_z^2}{k^2} \frac{4\pi q^2 n}{m} = \frac{k_z^2}{k^2} \omega_p^2 \tag{1.21}$$

where $\omega_p$ is the plasma frequency.

When the thermal pressure is included, the dispersion relation becomes:

$$\omega^2 = \frac{k_z^2}{k^2}\omega_p^2 + 3\overline{\mathrm{v}}^2 k_z^2. \tag{1.22}$$

Here the thermal pressure increases the mode frequency. The wave vector $k$ is equal to

$$k^2 = k_z^2 + k_\perp^2 \tag{1.23}$$

and in cylindrical geometry for $R_p \ll R_w$

$$k_\perp = \frac{1}{R_p}\left(\frac{2}{\ln(R_w/R_p)}\right)^{1/2}. \tag{1.24}$$

It is interesting to note that if we had kept all $k$ (not only $k_z$) we would get

$$\omega^2 = \omega_p^2(1 + \frac{3}{2}k^2\lambda_D^2) \tag{1.25}$$

which is the standard plasma wave dispersion relation for an infinite un-

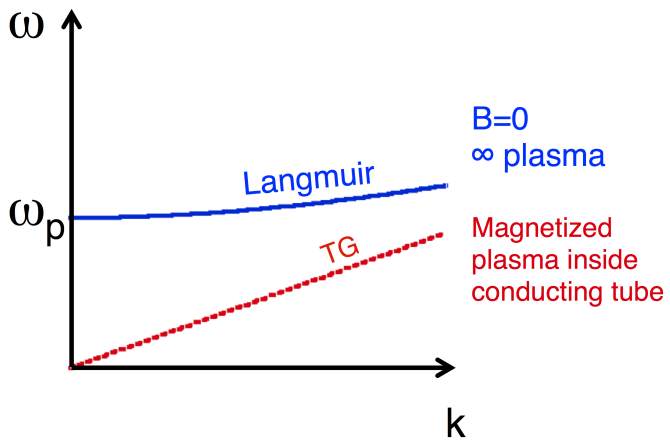


Fig. 1.7. Dispersion relation for Langmuir wave and Trivelpiece-Gould wave.

magnetized plasma, known in plasma physics as a Langmuir wave. The dispersion relation of these two types of plasma waves is shown on Fig. 1.7.

In an infinite, unbound plasma, when we have a little bit of extra charge $\delta q$ at one location and little deficit of charge at another location, an electric field $E$ is established. In contrast, when a plasma is inside a conducting

wall, the electric field $E_z$ is reduced by the conducting wall. At the wall $E_z = 0$ and only $E_r$ is not zero. This reduction of $E_z$ reduces the restoring force and therefore lowers the oscillation frequency; the frequency of plasma waves called Trivelpiece-Gould waves is lower than the frequency of plasma waves in an unbounded system called Langmuir waves ($f_{\rm TG} < f_{\rm Langmuir}$).

### 1.2.1. *Finite length Trivelpiece-Gould modes*

For trapped plasmas, the wavelength has to fit in the plasma such that the wave is reflected at each end of the trap, generating a standing wave with a parallel wave vector:

$$k_z = \frac{m_z \pi}{L_p} \tag{1.26}$$

where $m_z$ is the parallel mode number: $m_z = 1$ corresponds to one half wavelength in the plasma, $m_z = 2$ corresponds to a full wavelength in the plasma. In the limit of a long column ($k_z \lambda_D \ll 1$ and $R_p k_z \ll 1$), the frequencies of the axisymmetric ($m_\theta = 0$) Trivelpiece-Gould (TG) mode are:

$$\omega \cong \omega_p \left(\frac{R_p}{R_w}\right) (R_w k_z) \left[\frac{1}{2} \ln\left(\frac{R_w}{R_p}\right)\right]^{1/2} \left[1 + \frac{3}{2}\left(\frac{\overline{\rm v}}{{\rm v}_{\rm ph}}\right)^2\right] \tag{1.27}$$

for non-axisymmetric modes ($m_\theta \neq 0$).

$$\omega - m_\theta \omega_E = \omega_p \left(\frac{R_p}{R_w}\right) R_w k_z \frac{1}{j_{m_\theta, m_r}} \left[1 + \frac{3}{2}\left(\frac{\overline{\rm v}}{{\rm v}_{\rm ph}}\right)^2\right]. \tag{1.28}$$

Equation (1.28) assumed the mode frequency $\omega$ is of the same order as $m_\theta \omega_E$, which is valid for the ion case. In contrast for electron plasmas $\omega$ is large compared to the rotation $m_\theta \omega_E$. For electron plasmas the Bessel function zero $\gamma m_\theta, m_r$ of Eq. (1.28) is replaced by $\gamma m_{\theta-1}, m_r$.[13] These dispersion relations are "acoustic," with $\omega \propto k_z$, and all frequencies have the same phase (and group) velocity. The $m_\theta \neq 0$ modes are Doppler shifted by the plasma rotation frequency; these can be useful for some rotating wall applications.[14]

Experimental observations indicate that $k_z = m_z \pi / L_p$ is too large by about 10% and that the effective wavenumber corresponds to a longer wavelength extending past the end of the plasma. A theoretical model similar to an organ pipe wave number calculation gives: $k_{\rm eff} = k_z + \alpha_1 R_p + \alpha_2 R_W$, where $\alpha_1$ and $\alpha_2$ are given in Ref. 15.

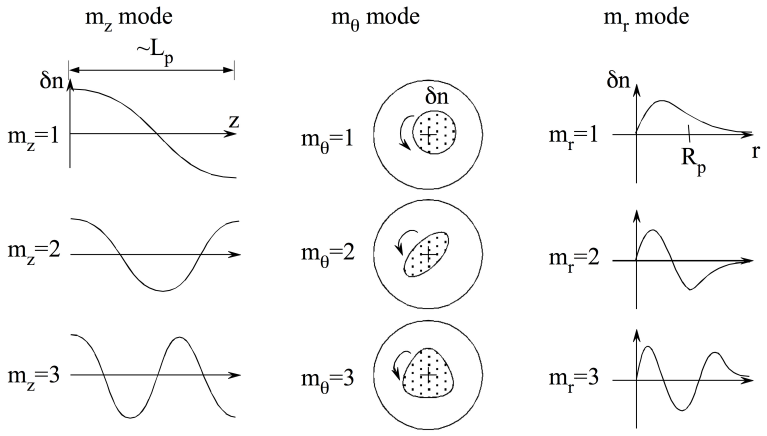


Fig. 1.8. Summary of longitudinal, azimuthal and radial wave number physical meaning.

Figure 1.8 summarizes all the $m$'s used to describe the TG plasma modes. Higher $m_z$ results in higher mode frequency; higher $m_\theta$ results in lower Doppler shifted mode frequency $\omega - m_\theta \omega_E$ and higher radial mode number $m_r$ results in lower mode frequency.

### 1.2.2. *Thermally excited Trivelpiece-Gould modes*

Trivelpiece-Gould (TG) modes are easy to excite. Figure 1.9 shows the results of a "transmission" experiment in a pure electron plasma; $m_z = 1$ to 5 are shown with a -80 dBm drive. As the drive amplitude is reduced, the received amplitudes are reduced, and $m_z = 2$ disappears into the noise, since the antenna geometry was not effective at detecting $m_z = 2$. More interestingly, when the drive amplitude is turned off, TG modes are spontaneously excited at low level by thermal fluctuations.[17]

As we will see, the thermal excitation of plasma modes provides an effective diagnostic tool; since non-neutral plasmas can relax to a state of thermal equilibrium in the rotating frame, the "tools" of thermodynamics can be used. The plasma mode is excited by thermal electron motion in the plasma and by noise in the load (i.e. measuring circuit). At the same time, the plasma mode is damped due to Landau damping and by dissipation in the load.

Nyquist's theorem quantifies the amount of thermal noise in a circuit

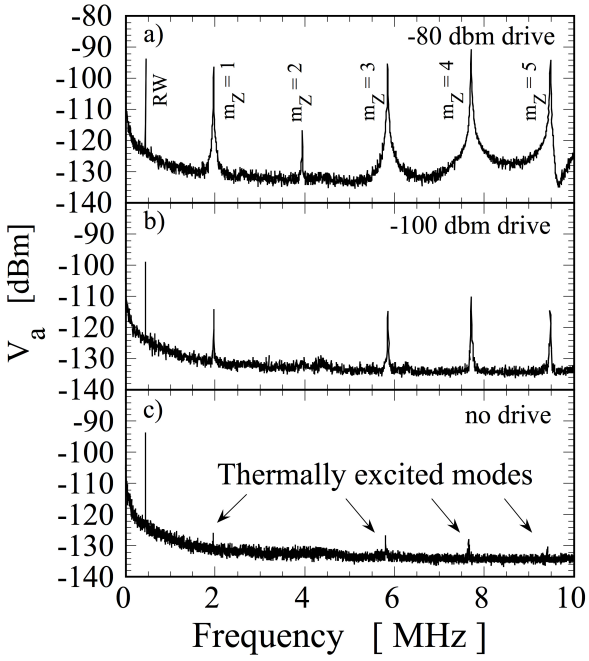


Fig. 1.9. Spectrum of $m_\theta = 1, 2, ..., 5$ Trivelpiece-Gould modes for three drive amplitudes including no drive, i.e. thermally excited.

element:

$$\frac{V^2}{df} = 4k_B T \, \mathrm{Re}(Z). \tag{1.29}$$

Figure 1.10 shows the electronic detection circuit attached to the electrodes

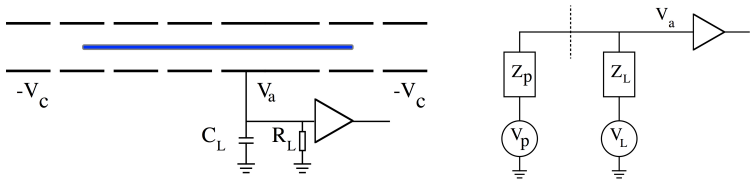


Fig. 1.10. Schematic diagram of Penning-Malmberg trap electrodes and electrical circuit analogue to plasma mode and receiver.

of trap, and the lump circuit element model. Applying the Nyquist theorem

to our trap, we get

$$\frac{V_a^2}{df} = \underbrace{4k_B T_p \,\mathrm{Re}(Z_p)\left|\frac{Z_L}{Z_p+Z_L}\right|^2}_{\text{plasma}} + \underbrace{4k_B T_L \,\mathrm{Re}(Z_L)\left|\frac{Z_p}{Z_p+Z_L}\right|^2}_{\text{load}} \tag{1.30}$$

where $V_a$ stands for the antenna voltage. The load impedance from a resistor and capacitor in parallel is $Z_L^{-1} = R_L^{-1} + i\omega C_L$. The plasma impedance around one mode is given by[16] $Z_p = G\omega_m^2/[i(\omega-\omega_m)+\gamma_m]$, where $G$ is a coupling coefficient due to the geometry, and $\gamma_m$ is the mode damping.

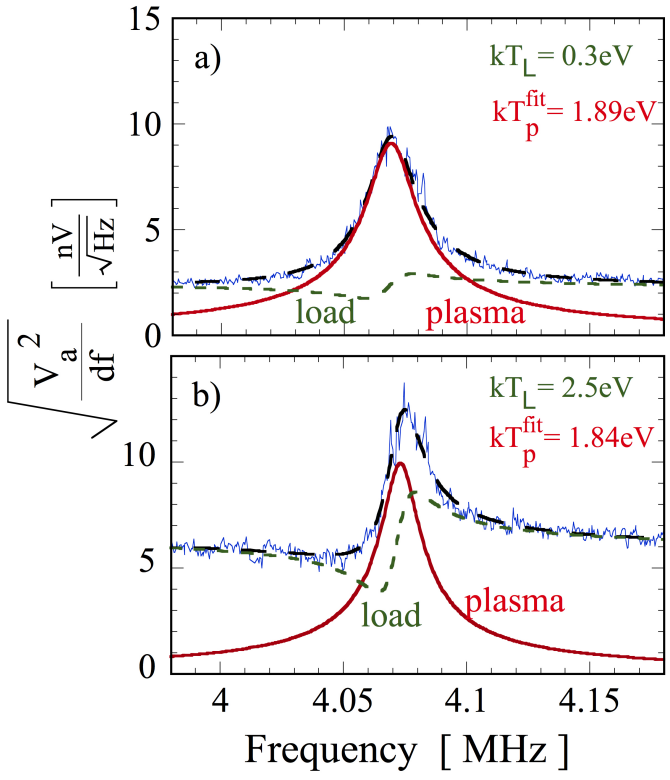


Fig. 1.11. Spectra of thermally excited TG mode for (a) $kT_{\mathrm{plasma}} = 1.89\mathrm{eV}$ and $kT_{\mathrm{load}} = 0.3\mathrm{eV}$; (b) $kT_{\mathrm{plasma}} = 1.84\mathrm{eV}$ and $kT_{\mathrm{load}} = 2.5\mathrm{eV}$. The long dashed line is Eq. (1.30) fitted to the data; the solid line is the plasma component and the short dashed line is the load noise filtered by the plasma.

The measured voltage fluctuations on the antenna are shown in

Fig. 1.11; the fluctuations are decomposed in two parts, a Lorentzian from the plasma, and a dip-and-step from the load. The red trace is from the Lorentzian plasma contribution and the green trace is from the thermal noise of the load. The temperatures of the plasmas and of the load are obtained from this decomposition. The temperatures of the plasmas measured by this "emission" technique are plotted on the vertical axis of Fig. 1.12 versus the temperatures measured by a standard slow dump of the particles contained in the trap. Here we used a room temperature amplifier to measure the thermally excited mode at plasma temperatures as low as 2.5 times room temperature. Figure 1.12 shows that both temperature diagnostics

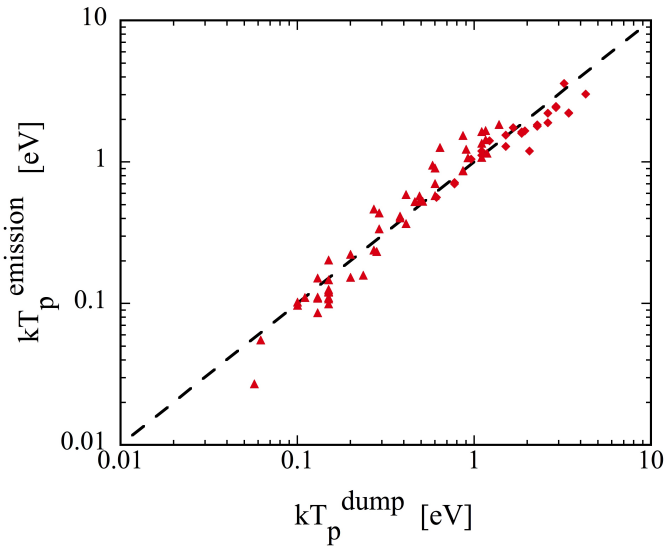


Fig. 1.12. Plasma temperature measured by emission technique versus standard dump temperature measurement. The two types of symbol represent measurements performed on two apparatuses.

agree within 15%, which is typical of the accuracy of the dump temperature diagnostic.

### 1.2.3. *Higher order Trivelpiece-Gould modes*

So far we have discussed axisymmetric plasma waves; here, I will be showing briefly some experimental results of plasma modes with azimuthal depen-

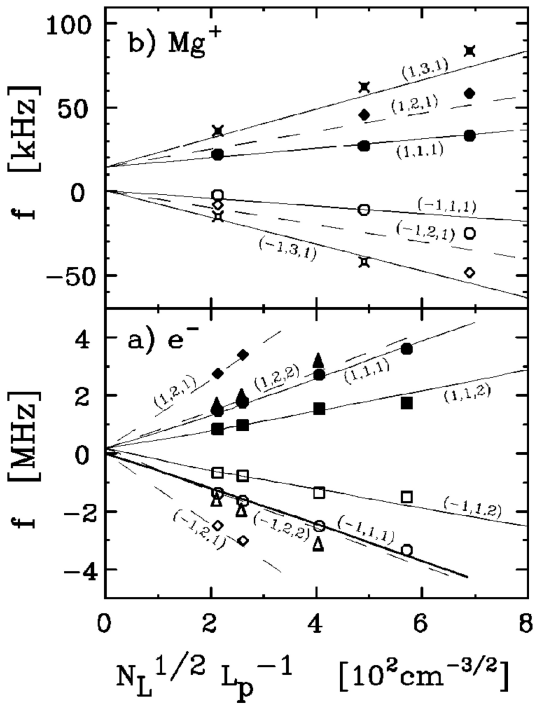


Fig. 1.13. Observed mode frequencies of $m_\theta = \pm 1$ as a function of plasma length $L_p$.

dance. Figure 1.13 shows the observed mode frequencies for azimuthal mode $m_\theta = \pm 1$ in a magnesium ion plasma, and in a pure electron plasma. The modes are Doppler-shifted according to Eq (1.28) by the plasma rotation frequency. The shift is clearly visible on the $Mg^+$ data, but is hard to see on the electron data, since the electron mode frequency is larger by a factor $\sqrt{m_i/m_e}$, whereas the rotation frequencies are comparable. Figure 1.13 demonstrates that the Doppler shifted mode frequencies are proportional to $N_L^{1/2} L_p^{-1}$.

### 1.2.4. *Electron acoustic waves*

Electron Acoustic Waves (EAW)[18,19] are plasma waves with a slow phase velocity, typically $\omega \approx 1.4 k\overline{v}$; in contrast, TG modes have $\omega \gtrsim 3k\overline{v}$. The name comes from the neutral plasma community: the ions are stationary,

as for electron plasma waves; but the mobile electrons give an acoustic response. Analogous EAW modes are observed in pure electron and pure ion plasmas (where the name is somewhat misleading). The EAW is non-linear so as to flatten the particle distribution to avoid strong Landau damping, but it can exist at small amplitude. Figure 1.14 shows the dispersion relation of plasma waves in an infinite size plasma where the dispersion relation has the shape of a "thumb."

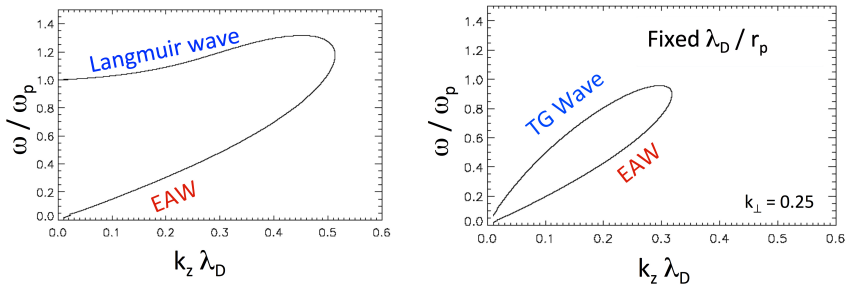


Fig. 1.14. Plasma wave dispersion relation in homogeneous infinite plasma and plasma of finite radial size.

In a trapped non-neutral plasma with a finite radial size $R_p$ resulting in $k_\perp$ given by Eq. (1.24), the dispersion curve looks like a "tear drop" when $\lambda_D/R_p$ is fixed. Experimentally it is easier to fix $k_z$ and $R_p$, measuring the dispersion curve as a function of temperature $T$ as shown in Fig. 1.15. The upper squares correspond to TG waves and the lower dots to EAW. At small amplitude ($A_{\rm exc} = 50$mV) no waves are observed for $T > 1.3$eV corresponding to $R_p/\lambda_D < 2$. The TG wave is easily excited with bursts as short as 3–10 cycles; in contrast the EAW requires typically hundreds of cycles to be excited. However, at larger amplitude the waves are excited over a range of frequencies. The bar at $T = 0.8$eV shows the range of frequencies over which a 100 cycle burst with $A_{\rm exc} = 300$mV results in a wave at frequency $f = f_{\rm exc}$ ringing for hundreds of cycles. This means that at $T = 0.8$eV, a wave can be excited at "any frequencies" within the vertical extent of the grey bar. Similarly, waves at $T = 1.4$eV are excited past the "end of the thumb," where no near-linear solution exists. For these off-dispersion relation waves, the drive modifies the particle distribution until the distribution becomes resonant with the drive.

We note that similar modes may occur in laser-plasma interactions, where they are called KEEN (Kinetic Electrostatic Electron Nonlinear)

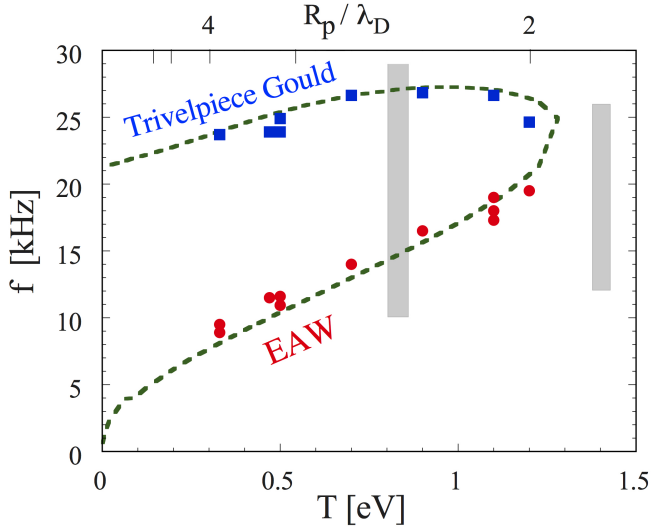


Fig. 1.15. Plasma wave dispersion relation for finite radial size plasma with fixed $k_z$ plotted versus temperature.

waves.[20] The connections between EAWs and KEEN waves are currently being investigated.

### 1.3. Cyclotron Wave

A single particle of charge $q$ and mass $m$ in a magnetic field has a cyclotron frequency $f_c = qB/(2\pi m)$. In a plasma, the cyclotron mode frequency is shifted from $f_c$. For a single species non-neutral plasma, cold fluid theory predicts that the cyclotron mode has frequencies:[21]

$$f = f_c + f_{E\times B}\left\{(m_\theta - 2) + \left[1 - \left(\frac{R_p}{R_w}\right)^{2m_\theta}\right]\right\}. \tag{1.31}$$

One can see that for $m_\theta = 1$ the cyclotron mode frequency is downshifted by one diocotron frequency. Figure 1.16 shows the measured cyclotron mode frequency of a pure electron plasma plotted against the diocotron frequency, demonstrating that for a single species plasma the lowest order cyclotron mode is downshifted by one diocotron frequency.

For multispecies non-neutral plasmas, cyclotron modes can be used to identify the composition of the plasma, but the exact frequency shifts are

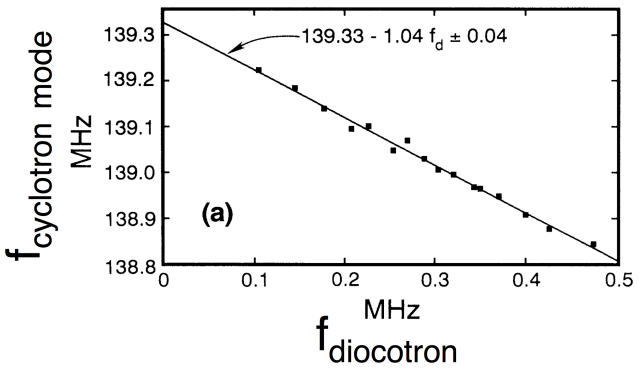


Fig. 1.16. Electron cyclotron mode frequency[21] plotted versus measured diocotron frequency. The solid line demonstrates the validity of Eq. (1.31) for single species plasmas.

still a work in progress.

## 1.4. Acknowledgments

This work was supported by National Science Foundation Grant PHY-9093877 and Department of Energy Grant DE-SC0002451. The author thanks the organizers of the Les Houches winter school for the opportunity to contribute to the workshop. The author also thanks Jo Ann Christina for typing and editing the manuscript, and Prof. C. F. Driscoll, Prof. D. H. E. Dubin, and Prof. T. M. O'Neil for many years of enlightened guidance and theory support.

## References

1. R. C. Davidson, *Physics of Nonneutral Plasmas*, Addison-Wesley (1990).
2. J. S. deGrassie and J. H. Malmberg, *Phys. Fluids* **23**, 63–81 (1980).
3. T. M. O'Neil, *Phys. Today* **52**, 24–30 (1999).
4. J. S. deGrassie and J. H. Malmberg, *Phys. Rev. Lett.* **39**, 1077–1080 (1977).
5. W. D. White, J. H. Malmberg and C. F. Driscoll, Resistive-wall destabilization of diocotron waves, *Phys. Rev. Lett.* **49**, 1822–1825 (1982).
6. K. S. Fine, *Experiments with the $l = 1$ Diocotron Mode*. Ph.D. Dissertation, UCSD Physics Dept. (1988).
7. C. .F. Driscoll, Observation of an unstable $l = 1$ diocotron mode on a hollow electron column, *Phys. Rev. Lett.* **64**, 645–648 (1990).
8. J. R. Danielson, T. R. Weber and C. M. Surko, Next generation trap for

positron storage, Non-Neutral Plasma Physics VII, *AIP Conf. Proc.* **1114**, 199–206 (1990).
9. K. S. Fine, C. F. Driscoll and J. H. Malmberg, Measurements of a nonlinear diocotron Mode in pure electron plasmas," *Phys. Rev. Lett.* **63**, 2232–2235 (1989).
10. K. S. Fine and C. F. Driscoll, The finite length diocotron mode, *Phys. Plasmas* **5**, 601–607 (1998).
11. S. A. Prasad and T. M. O'Neil, Waves in a cold pure electron plasma of finite length, *Phys. Fluids* **26**, 665–672 (1983).
12. A. W. Trivelpiece and R. W. Gould, *J. Appl. Phys.* **30**, 1784–1793 (1959).
13. A. A. Kabantsev and C. F. Driscoll, "Correction to electron plasma mode frequency formula," nnp.ucsd.edu/publications.html (2006).
14. F. Anderegg, E. M. Hollmann, and C. F. Driscoll, Rotating field confinement of pure elecron plasmas using Trivelpiece-Gould modes, *Phys. Rev. Lett.* **78**, 4875–4878 (1998).
15. J. K. Jennings, R. L. Spencer and K. C. Hansen, Numerical calculation of axisymmetric electrostatic modes for cold finite-length non-neutral plasmas, *Phys. Plasmas* **2**, 2630–2639 (1995).
16. N. Shiga, F. Anderegg, D. H. E. Dubin, C. F. Driscoll and R. W. Gould, Thermally excited fluctuations as a pure electron plasma temperature diagnostic, *Phys. Plasmas* **13**, 022109:1-12 (2006).
17. F. Anderegg, N. Shiga, D. H. E. Dubin, and C. F. Driscoll and R. Gould, Thermally excited Trivelpiece-Gould modes as a pure electron plasma temperature diagnostic, *Phys. Plasmas* **10**, 1556 (2003); F. Anderegg, N. Shiga, J. R. Danielson, D. H. E. Dubin, C. F. Driscoll and R. W. Gould, Thermally excited modes in a pure electron plasma, *Phys. Rev. Lett.* **90**, 115001:1-4 (2003).
18. J. P. Holloway and J. J. Dorning, Undamped plasma waves, *Phys. Rev. A* **44**, 3856–3868 (1991).
19. F. Valentini, T. M. O'Neil and D. H. E. Dubin, Excitation of nonlinear electron acoustic waves, *Phys. Plasmas* **13**, 052303:1-7 (2006).
20. B. Afeyan, K. Won, V. Savchenko, T. W. Johnston, A. Ghizzon, and P. Bertrand, in *Proc. of the Inertial Fusion Sciences and Applications 2003*, edited by B. A. Hamel, D. D. Meyerhofer, J. Meyer-ter-Vehn, and H. Azechi (American Nuclear Society, Monterey, 2004), p. 213.
21. R. W. Gould and M. A. LaPointe, Cyclotron resonance in a pure electron plasma, *Phys. Rev. Lett.* **67**, 3685–3688 (1991); R. W. Gould and M. A. LaPointe, Cyclotron resonance phenomena in a pure electron plasma, *Phys. Fluids B* **4**, 2038–2043 (1992); R. W. Gould, Theory of cyclotron resonance in a cylindrical nonneutral plasma, *Phys Plasmas* **2**, 1404–1411 (1995).